Biointerface Research in Applied Chemistry
Open-Access Journal (ISSN: 2069-5837)

Article
Volume 13, Issue 5, 2023, 411
https://doi.org/10.33263/BRIAC135.411

In silico study of selected lignins as COX-2 inhibitors

Loubna Taidi [1], Mohammed Reda Britel [1], Amal Maurady [2,*]

[1] Laboratory of Innovative Technology, University Abdelmalek Essaadi, Tetouan, Morocco; Taidiloubna_91@hotmail.fr (T.L.);
[2] Faculty of Sciences and Technologies of Tangier, University Abdelmalek Essaadi, Tangier, Morocco; amal.maurady.ma@gmail.com (M.A.);
* Correspondence: amal.maurady.ma@gmail.com (M.A.);

Scopus Author ID36011971000
Received: 7.06.2022; Accepted: 5.07.2022; Published: 17.11.2022

Abstract: Natural products present in medicinal plants play an important role in several biological processes, many of which alleviate and control inflammation-related diseases. These have been linked to an action involving direct inhibitory binding, especially on COX-2 protein. The present study reports the in-silico study of selected lignins for COX-2 inhibition and its correlation with its anti-inflammatory activities. We aim to understand lignin's structural and conformational features for inhibitory capability and illustrate their binding mode in the COX-2 active site. For this purpose, six lignins, namely pinoresinol, syringaresinol, 1-acetoxypinoresinol, berchemol, 8-Hydroxypinoresinol, and (-)-Olivil have been analyzed through ADME (absorption, distribution, metabolism, excretion) prediction, molecular docking study, molecular dynamic simulation, and binding free energy analysis. ADME study supports the potential biological activity of all selected lignins. At the same time, the described docking scores, the interaction profile, and the obtained conformations suggested berchemol as the best inhibitor for COX-2 protein, followed by 8-Hydroxypinoresinol and pinoresinol. 50 ns of the molecular dynamic simulation was then used to evaluate the stability of docked protein-ligand complexes and to estimate the conformational changes occurring during protein-ligand interaction. From the RMSD, RMSF, the number of hydrogen bonds, SASA, and MM/PBSA binding free energy score analysis, we have found that syringaresinol showed a good binding free energy score of -154.06±15.08 kJ/mol and displayed excellent pharmacological and structural properties to be drug candidate for the anti-inflammatory disease. In addition, MD results indicated shows that syringaresinol established more favorable interactions than rofecoxib. It is fixed in the COX-2 active site by the key residue Tyr-355 and stabilized by Ser-530.

Keywords: cyclooxygenase-2; inhibition; selectivity; lignins; ADME prediction; molecular docking; Lipinski rule of five; molecular dynamic simulation.

1. Introduction

Inflammation is the body's immune system's response associated with infection, irritation, and tissue injury[1]; however, in several cases, it can be implicated in the pathogenesis of diseases such as arthritis, cancer, atherosclerosis, stroke, and epilepsy, as well as neurodegenerative diseases [2]. The pathogenic process involves a number of inflammatory mediators, such as prostaglandins (PG), thromboxanes, and leukotrienes. The coordinated action of eicosanoid-forming enzymes controls the production of various prostaglandins from arachidonic acid called Cyclooxygenase (COX) [3]. Inhibition of prostaglandin synthesis is the

central mechanism by which Non-steroidal anti-inflammatory drugs (NSAIDs) reduce inflammation and pain in arthritis and other inflammatory conditions. For many years, this led to a nihilistic perception that there could be no therapeutic gain without the pain of gastrointestinal toxicity. This was changed by the discovery that there are (at least) two cyclooxygenase (COX) enzymes [4]. COX-1 is referred to as a constitutive isoform, and it has an important role in protecting the intestine, regulating and maintaining the plasma flow of the kidneys, and the glomerular filtration rate during a situation of vasoconstriction[5,6]. In contrast, COX-2 expression was found to be induced in response to various hormones, pro-inflammatory factors, growth factors, and oncogenes and inhibited by glucocorticoids [7].

NSAIDs constitute an important class of drugs with therapeutic applications that have spanned several centuries [8]. Their role is blocking the COX enzymes and reducing prostaglandins throughout the body; consequently, ongoing inflammation, pain, and fever are reduced [9]. Traditional NSAIDs that demonstrate nonselective COX inhibition, such as aspirin, ibuprofen, and diclofenac, are some of the most often recommended NSAIDs for the temporary relief of fever, pain, and inflammation[10,11]. These nonselective COX inhibitors were distinguished by the presence of a carboxylic acid (COOH) functional group. In the early 1990s, another isoform of COX was discovered, providing a new target for developing anti-inflammatory agents with a better safety profile compared to traditional NSAIDs [12]. Therefore, selective COX-2 inhibitors (coxibs) were developed as safer NSAIDs with betters gastric safety profiles[13,14]. These tricyclics compounds (coxibs) possess 1,2-diaryl substitution on a central hetero or carbocyclic ring system with a typical methanesulfonyl, sulfonamido, azido, methanesulfonamide, or pharmacophore-based tetrazole group on one of the aryl rings that plays a crucial role in COX-2 selectivity by orienting in a secondary pocket that is accessible only in the COX-2 active site [15,16]. Coxibs like Celecoxib, Rofecoxib, Valdecoxib, etc., belong to this common structural class [17]. However, reports of increased cardiovascular morbidity and mortality followed, and Merck manufacturer was forced to withdraw rofecoxib (Vioxx) from the market in 2004 [18]. Clinical studies have shown a link between using the sulfone cyclooxygenase (COX-2) inhibitor, rofecoxib, and increased risk of atherothrombotic events. This increased risk was not observed for a sulfonamide COX-2 inhibitor (celecoxib)[19]. The explanation for such cardiotoxicity is that rofecoxib forms a toxic metabolite that causes disruption in essential cellular structure-function relationships[20]. It is noteworthy that this reactive metabolite could not be derived from celecoxib, valdecoxib, and lumiracoxib due to their inability to form analogous chemical metabolites [21].

Moreover, it has been shown that in vitro the methylsulfone of rofecoxib increase the oxidative modification of human LDL through a non-enzymatic process, whereas other coxibs (celecoxib, valdecoxib, meloxicam) and nonselective COX inhibitors (ibuprofen, naproxen, diclofenac) had no effect [22]. From this bibliographical study, it seems that the higher the specificity towards COX-2 inhibition, the higher the risk of cardiovascular side effects. This observation is supported by the fact that celecoxib, which is the least COX-2 specific of all coxibs, is the only coxib that is still approved by the US Food and Drug Administration (FDA) [23].

Considering this, we aimed in this study to obtain natural molecules that inhibit the production of PGs generated from COX-2 and keep those produced by COX-1. To this effect, we set out to mimic the pharmacological profile of coxibs that have a diaryl heterocyclic backbone characterized by the presence of a cyclic functional group attached to two aromatic rings [24], with the aromatic rings having a new functional group (alcohol and ester) to define

a new mode of interaction in the COX-2 active site. The structure of pinoresinol, syringaresinol, berchemol, 8-Hydroxypinoresinol, and (-)-Olivil, which are lignins extracted from olive oil, contain these features, as shown in Figure 1.

In inflamed cells, pinoresinol significantly reduced cyclooxygenase (COX-2) derived prostaglandin E2 by 62% in confluent cells [25]. A previous study showed that syringaresinol potently inhibitedPGE2 production and COX-2 expression [26]. 8-Hydroxypinoresinol inhibited the production of inflammatory mediators, such as COX-2 and PGE2, in LPS-induced inflammation in RAW 264.7 cells [27]. On the other hand, another study revealed that pinoresinol induces potent tumoricidal effects by selectively triggering a large number of apoptotic cells[28]. In comparison, another study suggests that phenolic compounds isolated from rhizomes and roots of Gentianascabra showed that berchemol was potentially inhibitors EH activity [29]. The interest in lignin has increased due to its potential applications in some pharmacological applications, such as anti-tumor, anti-virus, antioxidant, anti-inflammatory, and antimicrobial activities[30,31].

In this study, we use in silico methods to study the potential of six lignins to inhibit COX-2 activity. Pinoresinol, syringaresinol, 1-actoxypinoresinol, berchemol, 8-Hydroxypinoresinol, and (-)-Olivil were selected and were subject to calculate their pharmacokinetic properties such as Lipinski's rule of five and ADME parameters. Structure-based analyses were performed to evaluate the Root Mean Square Deviation and Fluctuations (RMSD/F), hydrogen bond profile, Solvent Accessible Surface Area (SASA), and binding free energy score calculations using the MMPBSA method, to verify their behavior when bound to COX-2 active site.

2. Material and Methods

2.1. Biomolecules.

To optimize the activity of COX-2 inhibitors and therefore, to reduce their systemic toxicity, we have chosen to retain the basic structure of coxibs as a pharmacophore for the search for natural molecules. The coxibs are chemically characterized by the presence of a bulky structure comprising 2 large aromatic rings linked to a central heterocycle [32]. Coxibs must contain three functions, as shown in Figure 1. Modulating the groups R1, R2 and R3 makes it possible to affect the molecules' bioavailability, affinity, and specificity.

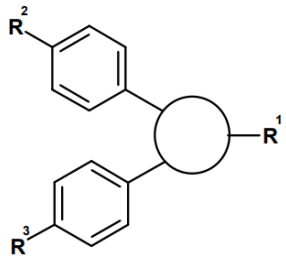

Figure 1. 2D structure of Coxibs.

Lignins present antimicrobial and antioxidant properties. The antimicrobial properties of lignins are due to the phenolic groups contained in their structure. These phenolic groups are known to damage the bacterial envelope and subsequently generate cell lysis and liberate the cellular components. The antioxidant activity of lignin is also positively correlated with the number of phenolic groups as they act as hydrogen donor antioxidants. Low molecular weight,

low number of aliphatic hydroxyl groups, and low heterogeneity also appear to enhance the antioxidant activity of lignins.

Furthermore, it has been reported that lignins exhibit low cytotoxicity. Therefore, considering all these factors, lignins are a material with high potential to be used for the research of biomolecules inhibiting the activity of COX-2 protein [33]. In this study, we investigated the structure of lignins extracted from olive oil since it is a major component of the Mediterranean diet, including 31.2% of lignins [34]. We have focused our studies on two articles which are based on the extraction and purification of existing lignins in olive oil to find lignins presenting some similarity to coxibs structure, with the presence of aromatic rings having a new functional group (alcohol and ester) to define a new mode of interaction in the COX-2 active site.

2.2. Lipinski's rule of five parameters.

Lipinski's rule of five describes molecular properties important for a drug's physicochemical properties in the human body, including their absorption, distribution, metabolism, and excretion [35]. Lipinski's rule of five parameters can filter a library of molecules and remove those predicted to have poor properties [36]. Drug candidates will be predicted to be absorbed from the intestine with respect to the following criteria [37]:

- To have a molecular weight of ≤ 500;
- a LogP (logarithm of the partition coefficient) ≤ 5;
- no more than five hydrogen bond donors;
- no more than ten hydrogen bond acceptors;
- number of rotatable bonds (nRotb) ≤ 10;

Based on these physicochemical requirements, not more than one of them should be violated. Molecules violating these rules may have problems with bioavailability [38]. The analysis was carried out to find whether the newly proposed compounds obeyed this rule using the Molinspiration server (https://www.molinspiration.com/).

2.3. ADME properties.

The efficacy and safety of a drug compound are determinant factors in bringing it into the market, and these factors can be considered through absorption, distribution, metabolism, and excretion (ADME) profiling [39]. ADME properties play an important role as they are responsible for the failure of 60% of drug molecules. Early prediction of these properties can help to a significant cost reduction in the field of drug research [40].

To study the absorption of a drug in the human body, the human colon carcinoma cell permeability test (Caco-2) has become one of the standard tools[41,42]. To classify the compounds for therapeutic purposes according to this last parameter, many laboratories use the following criteria: Values <20 nm/s predict low transcellular absorption in vivo (fraction of 0 to 20% absorbed); values between 20 - 80 nm/s predict moderate transcellular absorption in vivo (20 to 80% of the absorbed fraction) and values between 80 and 100 nm/ s predict strong transcellular absorption in vivo (80 to 100% of the fraction absorbed fraction) [43].

The blood-brain barrier is a membrane that regulates the passage of substances from the blood to the central nervous system (CNS), acting on the fraction of the drug that reaches the brain [44,45]. The BBB can be considered an interface that maintains optimal conditions for neuronal and glial function by regulating the exchange of substances between the blood and

the brain [46]. Brain capillaries form this interface, rendering the brain inaccessible to polar molecules, except in cases where the molecules are transported by transmembrane proteins [46,47].

Cytochrome P450 enzymes are essential for the metabolism of many drugs. Although this class has more than 50 enzymes, CYP3A4 and CYP2D6 metabolize 90% of drugs. These enzymes are mainly expressed in the liver but are also present in the small intestine (reduced drug bioavailability), lungs, placenta, and kidneys [48]. Evaluating the interaction of CYP with chemicals is a fundamental step in drug discovery and design. For this reason, CYP3A4 and CYP2D6 of cytochrome P450 have been the target of numerous modeling studies [49].

The two main routes of excretion are via the kidneys and the liver, respectively. Clearance (Cl) is the parameter used to measure drug elimination. It is the result of elimination by renal excretion and extrarenal pathways (non-renal clearance), usually hepatic metabolism [50]. The units of clearance are the volume per unit of time. Therefore, clearance represents the volume of blood (or plasma) from which the drug has been completely cleared per unit of time [51].

In this study, the absorption, distribution, and metabolism properties of the selected lignins were estimated by the preADMET online database (https://preadmet.bmdrc.kr/). Clearance was estimated using the DruMAP online database (https://drumap.nibiohn.go.jp/).

2.4. Validation of molecular docking studies.

Redocking is performed as a validation method for all docked protein-ligand complexes. The three-dimensional structures of crystal rofecoxib are obtained by removing it from protein crystallographic complexes (5KIR). The crystal rofecoxib is then redocked with COX-2 proteins using AutoDock/VinaPyMol plugin. Root Mean Square Deviation (RMSD) value between crystal ligand and the best pose obtained from Autodock vina were calculated using Pymol software (http://www.pymol.org/). A maximum threshold of 2Å is used to discriminate between good and bad positions [52].

2.5. Molecular docking study.

The molecular docking study of the selected compounds into the COX-2 active sites was performed using the PyMol molecular visualization platform with AutoDock/Vina PyMol plugin. Human COX-2 was used as the target protein for molecular docking studies. The crystal structure of COX-2 (PDB ID; 5KIR) was obtained from the protein data bank (PDB). The 3D structures of the selected lignins were downloaded from PubChem (https://pubchem.ncbi.nlm.nih.gov) in SDF format and then converted into PDB files with OpenBabel, and then the resulting PDB files were subject to an optimization of the geometry and the coordinates using amber force field (GAFF) into mol2 format. The docking was performed for each ligand with an 'exhaustiveness' option set to 100 in the AutoDock Vina.

Grids were created utilizing informations on the crystal structure and molecular docking information on the native rofecoxib bound into the COX-2 protein and from the information previously described in the literature. So, the active site that include His-90, Arg-120, Gln-192, Val-3, Tyr-355, Leu-352, Ser-353, Leu-384, Tyr-385, Arg 513, Ala-516, Ile-517, Ala-527, Phe-518, Met-522, Val-523, Gly-526 and Ser-530[53–56]. Grids were cantered with x, y, and z coordinates with 23.21 1.32 34.26, and the size of each box was set to 60, 60, and 60. Autodock tools (ADT) package was employed to produce grids and docking parameter files

gpf and dpf. A 2.0 Å clustering tolerance was applied to construct clusters of the closest compounds, and the initial coordinates of the ligand were used as the reference structure. Finally, the structures were ranked by energy.

2.6. Molecular dynamics simulation studies.

Molecular dynamics simulation (MD) was performed using GROMACS 2019.3 to extend the information on the stability and interaction profile of the selected lignins and rofecoxib with the COX-2 enzyme. The following protocols were used to perform the MD simulation. First, each protein-ligand complex was again prepared. For this simulation, PlayMolecule (https://www.playmolecule.org/proteinPrepare/), a web Application for protein preparation for molecular dynamics simulations, was used to prepare the structure of COX-2 enzyme for MD simulations by optimizing the hydrogen bond network and titrating the residues at physiological pH (pH=7.4). The Amber ff14SB force field was used for the protein parameters, and the antechamber program of the AmberTools19 package, in combination with the general amber force field GAFF was used to assign atom types and bonded parameters to the ligands. To neutralize the charge of the systems, two sodium ions were added to each system, and the protein was solvated with 16940 water molecules using the TIP3P water model in a box of about 12 Å. The system topologies were finally prepared with the tleap tool from the AmberTools19 software package and then translated to Gromacs topology files via ACYPE. Next, 50000 steps of steepest descent minimization were used for each complex before being used as the initial conformation for the equilibration (500 ps for NVT heating from 100 K to 310.15 K, followed by 500 ps for NPT) by applying the position restraints on protein and inhibitor with periodic boundary conditions (PBC). Short-range electrostatic interactions were cut-off at 1.4 nm, and long-range electrostatic interactions were evaluated using the particle mesh Ewald (PME) algorithm. Simulations were run with a 2 fs time step with the Berendsen algorithm to keep temperature and pressure constant. Bond lengths were constrained with the LINCS algorithm. Finally, the system was subjected to 50 ns MD at a temperature of 310.15 K and a pressure of 1 bar.

Dynamic behavior and stability of each residue were also analyzed, including root-mean-square deviation, root means square fluctuation, solvent accessible surface area, and hydrogen bond profile using Gromacs inbuilt tools.

2.7. Calculation of binding free energy.

In the computational drug discovery process, the free energy calculation analysis is important, because it gives a quantitative estimation of the binding free energy, which reflects the stability of the protein-ligand complex. To determine the total binding free energy, the free solvation energy (polar + non-polar solvation energies) and potential energy (electrostatic + Van der Waals interactions) of each protein-ligand complex were evaluated in the Molecular Mechanics Poisson–Boltzmann Surface Area (MM-PBSA) method. The last 10 ns of the MD trajectory were taken for the calculation of MM-PBSA. As g_mmpbsa only reads the files of some specific Gromacs versions, the binary run input file required for MM-PBSA calculation via the g_mmpbsa was produced by Gromacs 5.1.2. The molecular structure, topology, and MD parameter files were necessary to create the binary run input file, and they all came from the MD process.

3. Results and Discussion

3.1.Biomolecules.

The structure of lignins extracted and isolated from olive oil highlighted six lignins namely: pinoresinol (CID: 73399), syringaresinol (ID: 100067), 1-acetoxypinoresinol (ID: 442831), berchemol (ID: 14521044), 8-Hydroxypinoresinol (ID: 3010930), (-) - Olivil (ID: 5273570) (Figure 2) [57,58]. These lignins present an important structure that can be exploited to inhibit COX-2 activity. Extraction of the 3D structure of the selected compounds was done using the Pubchem database (https://pubchem.ncbi.nlm.nih.gov/).

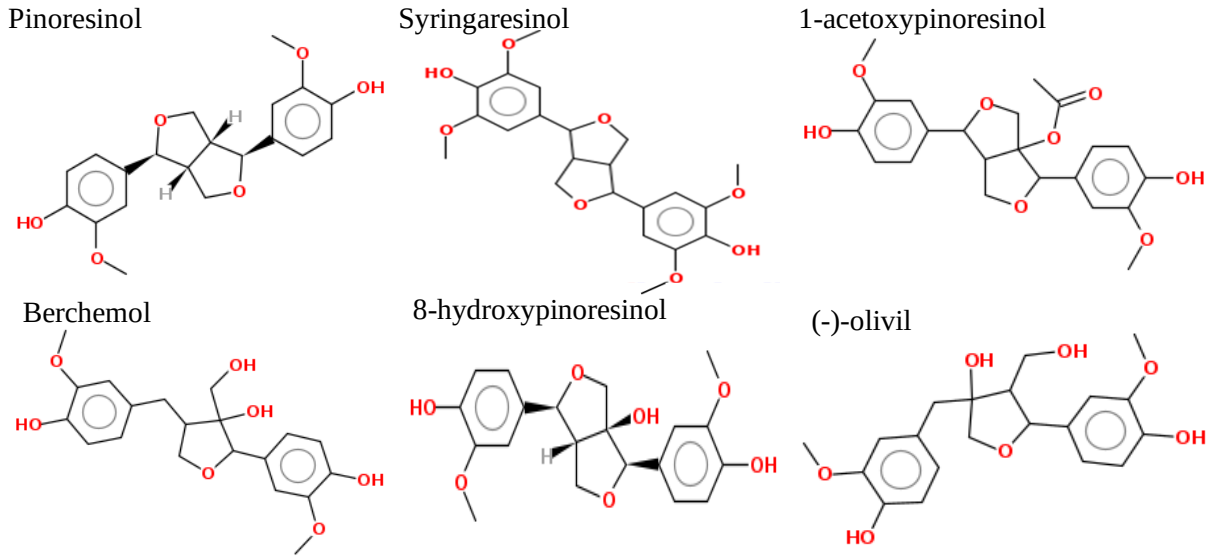

Figure 2. 2D chemical structures of the selected lignins.

3.2. Lipinski's rule of 5.

The physicochemical properties of selected compounds, as well as rofecoxib, were based on Lipinski's rule of five. Selected lignins under study, as well as rofecoxib, showed good results when analyzed using Lipinski's rule of 5 with 0 violations. Results shown in Table 1 revealed that all Lipinski's parameters are qualified; therefore, we can conclude that the selected lignins can increase their chances of becoming a drug.

Table 1. Summary of drug-like properties of the selected lignins and the rofecoxib based on Lipinski's rule of five.

NO	Ligand	logP	H-acc	H-don	MW	nRotb	NV
1	Pinoresinol	2.59	6	2	358.39	4	0
2	Syringaresinol	2.62	8	2	418.44	6	0
3	1-Acetoxypinoresinol	2.35	8	2	416.43	6	0
4	Berchemol	1.39	7	4	376.40	6	0
5	8-Hydroxypinoresinol	1.64	7	3	374.39	4	0
6	(-)-Olivil	1.39	7	4	376.40	6	0
7	Rofecoxib	0.71	4	0	314.36	3	0

logP: the octanol/water partition coefficient; **H-acc**: hydrogen bond acceptor; **H-don**: hydrogen bond donor; **MW:** molecular weight; **nRotb:** number of rotatable bonds; **NV:** number of violations.

3.3. ADME properties.

The favorable pharmacokinetic properties that should result in good absorption, distribution, metabolism, and excretion (ADME) are also considered important to the

molecules. A poor ADME profile can be a reason for clinical trial failure. Thus, early and accurate ADME profiling during the discovery phase is necessary to successfully develop candidate small molecules.

The ADME results in Table 2 show that the Caco-2 cell line permeability values obtained for lignins and rofecoxib range from 20 to 39 nm / s (4 ~ 70), meaning that all the compounds are predicted to be moderately permeable. On the other hand, the values of BBB demonstrate that all lignins as well as rofecoxib have an inactive CNS (central nervous system) of less than 1. The obtained values range between 0.02 and 0.14, indicating that these compounds may be less likely to cause side effects in the central nervous system.

Cytochrome P450s is an important enzyme for drug metabolism in the liver. The two main cytochrome P450 subtypes are CYP2D6 and CYP3A4. The results showed that lignins and rofecoxib were neither substrates nor inhibitors for CYP2D6, they are predicted to be inhibitors for CYP3A4. In addition, berchemol, 8-hydroxypinoresinol, (-)-olivil,and rofecoxib are predicted to be weak substrates for CYP3A4, while pinoresinol, syringaresinol, and 1-acetoxypinoresinol are predicted to be substrates for CYP3A4. This suggests that pinoresinol, syringaresinol, and 1-acetoxypinoresinol may be metabolized in the liver.

Drug elimination is related to the molecular weight and hydrophilicity of compounds. The prediction results show that the hepatic clearance of syringaresinol is the highest.

Table 2. preADMET prediction of selected lignins and rofecoxib.

Property / Model	A	D	M				E	
	Caco-2 nm/s	BBB	CYP3A4		CYP2D6		CL_h	CL_r
			Substrate	Inhibitor	Substrate	Inhibitor		
Pinoresinol	35.13	0.07	Substrate	Inhibitor	Non	Non	25.15	0.04
Syringaresinol	39.30	0.02	Substrate	Inhibitor	Non	Non	51.26	0.03
1-Acetoxypinoresinol	27.75	0.02	Substrate	Inhibitor	Non	Non	16.52	0.06
Berchemol	20.75	0.14	Weak	Inhibitor	Non	Non	14.75	0.00
8-Hydroxypinoresinol	22.79	0.09	Weak	Inhibitor	Non	Non	20.88	0.00
(-)-Olivil	20.75	0.13	Weak	Inhibitor	Non	Non	12.40	0.02
Rofecoxib	2.72	0.01	Weak	Inhibitor	Non	Non	6.13	0.00

Caco-2*:* Human Colon Carcinoma Cell *Line;* **BBB:**Blood–Brain Barrier Permeability*;* **CYP3A4:** CytochromeP450 3A4**; CYP2D6:** Cytochrome P450 2D6**; CL_h:** Hepatic clearance**; CL_r:** Renal clearance.

3.4. Redocking as a docking validation method.

The re-docking method was used to determine how closely the lowest binding energy pose resembles the experimental binding mode determined by X-ray crystallography. In the current study, after analyzing 100 conformations for rofecoxib, the results showed that Vina was able to recover the crystallized conformation with an RMSD of 1.466 Å. On the other hand, the alignment of the docked rofecoxib with the crystal one for visual analysis is an essential step in confirming the results of the RMSD test. It shows whether the simulated placement of a ligand is superimposed on the reference one. In our case, Figure 3 shows that we have a good superposition of rofecoxib simulated by Vina (colored in green) and those of the crystallized ligand (colored in blue). This test further confirms the test of RMSD, hence and the performance of the chosen software.

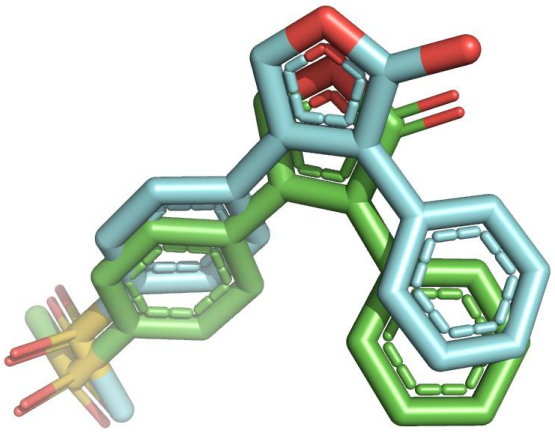

Figure 3. Superposition of re-docked rofecoxib (in green) with crystal ligand (in blue).

3.5. Pymol/Autodock vina plugin results.

The active site of COX-2 is split into three subdomains, as shown in Figure 4 (subdomain A, B, and C); the first is a hydrophobic pocket that is defined by Tyr-385, Trp-387, Phe-518, Ala-527, Ala-201, Tyr-248, and Leu-352; the second region is the active site entrance lined with the hydrophilic residues Arg-120, Val-349, Glu524 and Tyr355 and the third is the side pocket lined by His-90, Gln-192, Arg-513 and Val-523 [59]. For the selective COX-2 inhibitors like rofecoxib, the phenyl ring was in close proximity to the hydrophobic pocket, and the phenyl sulphonamide group occupied the side pocket and showed binding with important residues in the binding of selective COX-2 inhibitors Gln-192 and Ile-517. The results are consistent with the literature reports on the docking of selective COX-2 inhibitors [60]. One of the keys to the development of COX-2 selective drugs is the larger active site of COX-2, which allows to the synthesis of molecules able to fit the COX-2 [61].

Based on the "binding energy" parameter and the "interaction profile" shown in Table 3, berchemol was found to have the most favorable energy among the six lignins analyzed, followed by 1-Acetoxypinoresinol, (-)-Olivil, 8-Hedroxypinoresinol, pinoresinol, and syringaresinol.

Table 3. Summary of binding energy and interactions profile of COX-2 with the selected lignins and rofecoxib.

Ligand	ΔG (kcal/mol)	H-bond
Rofecoxib	-10.3	Gln-192, Ile-517, Phe-518
Berchemol	-9.71	Gln-192, Val-349, Ser-353, Phe-518
1-Acetoxypinoresinol	-9.02	Arg-120, Val-349, Tyr-385,
(-)-Olivil	-8.63	Gln-192, Val-349, Ile-517, Phe-518, Ser-530
8-Hydroxypinoresinol	-8.46	Arg-120, Tyr-385, Ser-530
Pinoresinol	-8.38	Arg-120, Val-349, Tyr-385
Syringaresinol	-8.23	Arg-120, Met-522

The rest of the study compares conformations obtained for lignins with that of rofecoxib. This choice is not fortuitous, but it will consolidate the docking results by inserting, into the binding site, the biomolecules resulting from the study carried out. The remarkable activity of selective COX-2 inhibitors is related to their stability, which is explained by the interaction with the key amino acids Arg-120, Tyr-355, Gln-192, His-90, Phe-518, Ser-530, Val-349, Val-523, Met-522, Ile-517. We present below the illustrations of the binding modes of the six lignins and rofecoxib in the COX-2 active site.

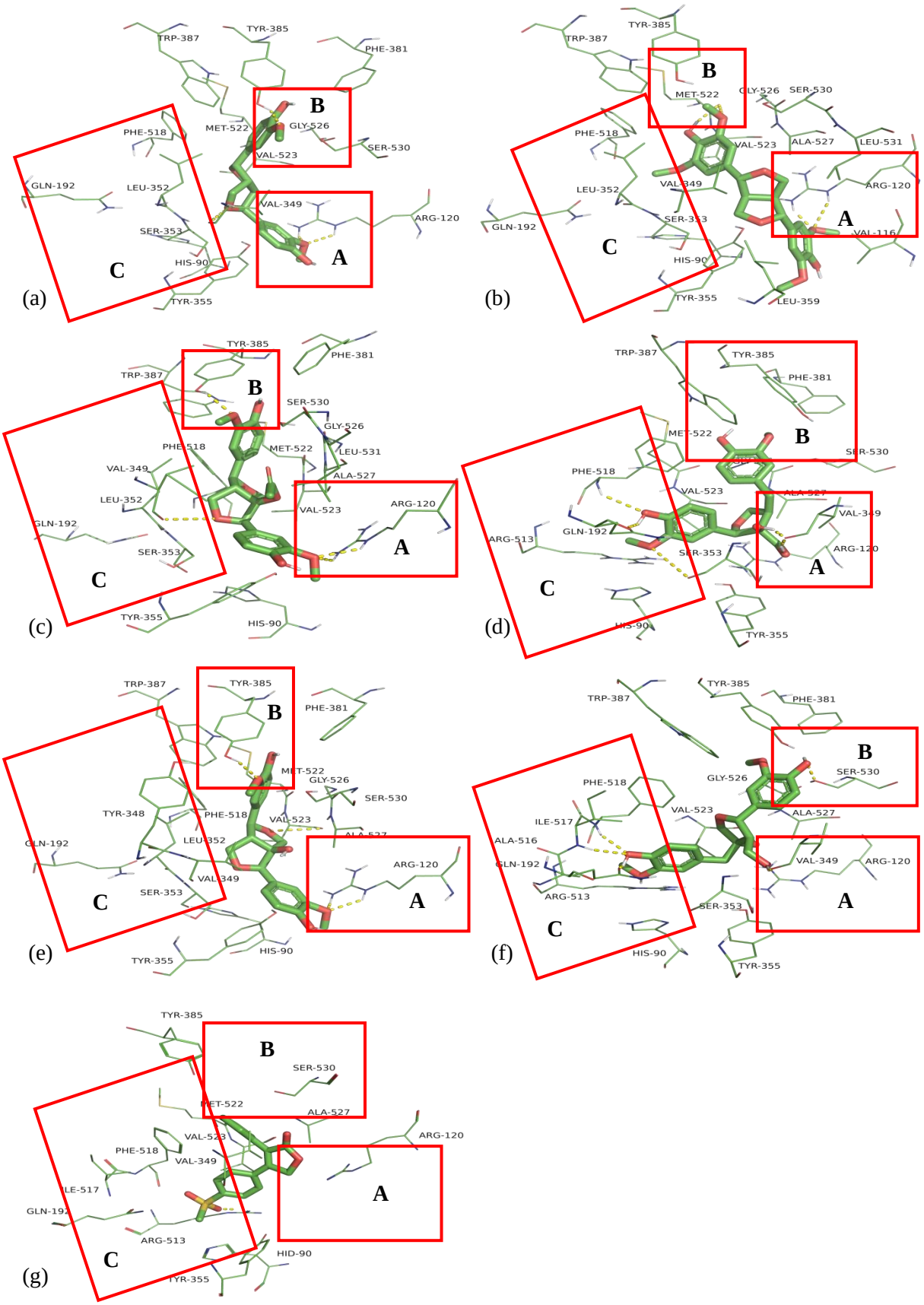

Figure 4. Docked compounds in COX-2 active site: (a), (b), (c), (d), (e),(f) and (g) respectively for pinoresinol, syringaresinol, 1-acetoxypinoresnol,berchemol, 8-Hydroxypinoresinol, (-)-Olivil and rofecoxib.

The illustration of berchemol in the COX-2 active site shows that this compound presented a good conformation. Its flexible structure allowed it to occupy the three domains of the COX-2 active site (the entrance to the site (A), the hydrophobic pocket (B), and the side chain (C)) as shown in Figure 4(d), and consequently to create hydrogen bonds with Gln-192, Val-349, Ser-353, Phe-518. On the other hand, pinoresinol, with a binding energy of -8.38 kcal/mol, was able to interact with the key residues Arg-120, Val-349, and Tyr-385, as shown in Figure 4(a) and therefore occupy the three domains of COX-2 active site. Moreover, 1-acetoxypinoresinol, 8-Hydroxypinoresinol, and (-)-Olivil, with binding energies of -9.02, -8.46, and -8.63 kcal/mol, respectively, had the same conformation in COX-2 active site (Figure 4 (c), (e) and (f)). These three lignins were unable to interact with lateral pocket residues such as berchemol, pinoresinol, and rofecoxib. Their structures allow the creation of hydrogen bonds with the residues of the entry of the active site, in particular with Arg-120, and with the residues of the hydrophobic pocket, such as Ser-530 and Tyr-385. Finally, the illustration of syringaresinol in the active site of COX-2 shows that it occupied two domains, as in the case of 1-acetoxypinoresinol, (-)-Olivil, and 8-Hydroxypinoresinol, but with another conformation which allowed, with a binding energy of -8.23 kcal/mol, to interact with a binding residue (Arg-120) and with a residue of the hydrophobic pocket (Met-52) (Figure 4(b)).

The results of this study show that among the lignins studied, berchemol and pinoresol are the only ones that occupied the entire active site of COX-2 by interacting with key amino acids.

3.6. Molecular dynamics studies

To verify the stability of our best docking positions, we performed molecular dynamics simulations. During molecular docking study, the flexibility of the protein is not taken into account, and only the ligand is flexible. Molecular dynamics makes it possible to access the most stable conformation (lowest in energy) from a docking position (ligand-protein complex obtained by molecular docking) by attributing certain flexibility to the ligand and the protein. For each of our ligand-protein complexes obtained by docking, we performed a minimization followed by a dynamic of 50 ns, and various geometric descriptors such RMSD, RMSF, and solvent accessible surface area (SASA) were determined.

3.6.1. Root mean square deviation (RMSD)

The stability of all systems was analyzed based on root mean square deviation (RMSD). For all systems, the RMSD profiles were determined after 50 ns of the MD simulation for the backbone atoms and for the heavy atoms of residues within 4 Å of the ligands. The backbone atoms of COX2- rofecoxib shows stability during the simulation, with an average RMSD of 0.25 ± 0.04 nm (Figure 5 (g)). In the case of the lignin, COX2-syringaresinol, COX2-berchemol, and COX2-(-)-olivil systems show great stability during the simulations and present RMSD much better than that presented by the COX2- rofecoxib system, with an average RMSD of 0.19 ± 0.02 nm, 0.21 ± 0.02 nm, and 0.14 ± 0.01 nm respectively. On the other hand, although COX2-pinoresinol, COX2-1-acetoxypinoresinol, and COX2-8-hydroxypinoresinol systems show favorable RMSD values of 0.19 ± 0.02 nm, 0.21 ± 0.02 nm, and 0.18 ± 0.03 nm respectively, but the graphical representations in Figure 5 (a), (c) and (e) show that they were unable to achieve stability throughout the simulation.

On the other hand, the average RMSD values between 0.12 and 0.20 nm for the heavy atoms of the surrounding residues of the ligands do not show a significant deviation of the overall structure of the enzyme from the X-ray data. Still, the graphical representations show that the active site of the syringaresinol, berchemol, 1-acetoxypinoresinol, and (-)-olivil systems are the most stable.

The RMSD results of the backbone atoms and residues of the COX-2 active site demonstrate that there is no important difference in conformation due to the binding of syringaresinol, berchemol, and (-)-olivil in the COX-2 active site.

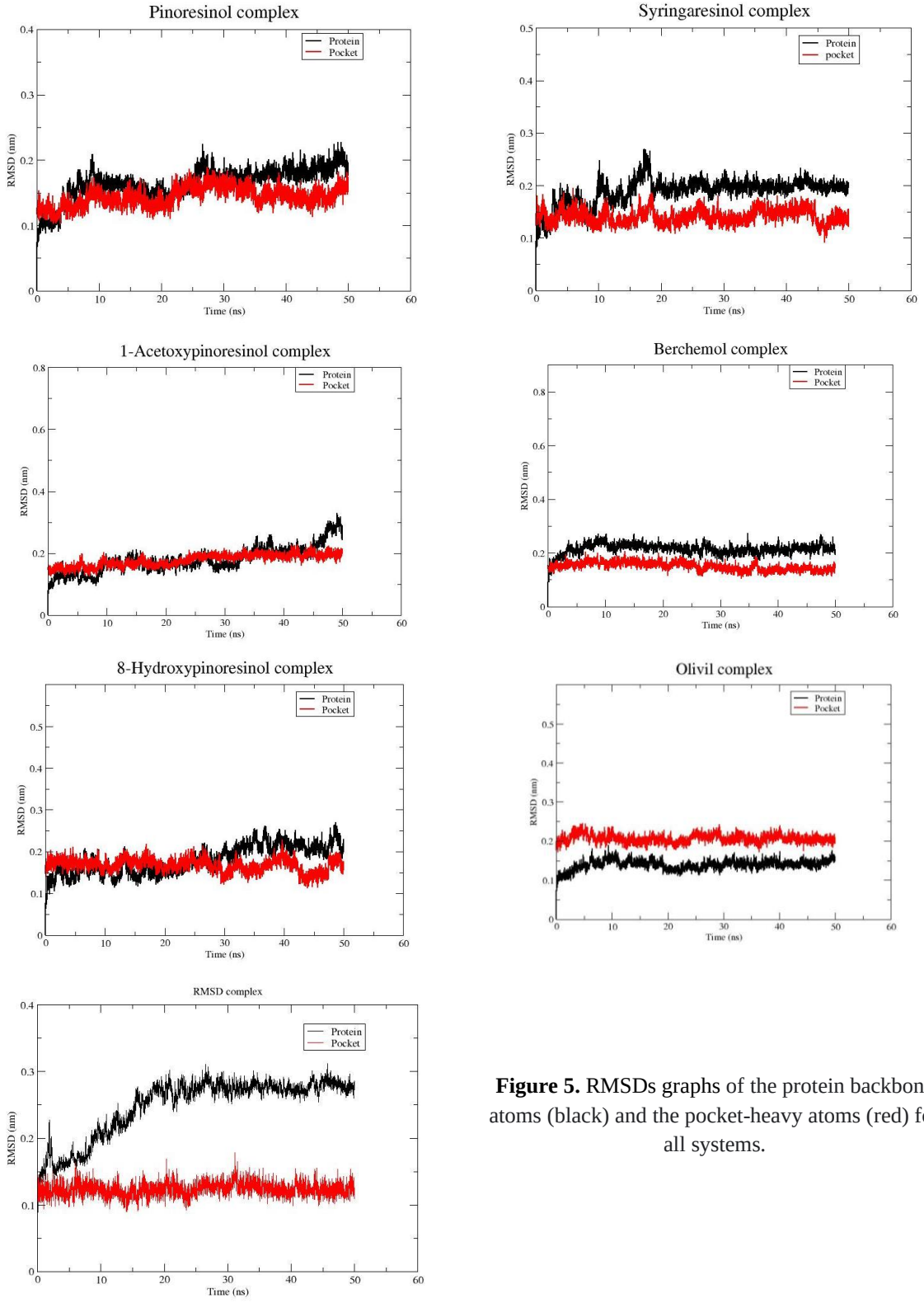

Figure 5. RMSDs graphs of the protein backbone atoms (black) and the pocket-heavy atoms (red) for all systems.

3.6.2. Root mean square fluctuation (RMSF)

The Root Mean Square Fluctuation (RMSF) is vital in analyzing local changes of the protein chain residues and in analyzing changes in the ligand atom positions at specific temperatures and pressure. The results presented in Figure 6 provide an overview of the main flexible regions of COX-2 protein. The results showed that the enzyme has different flexible regions due to their large RMSF values. The fluctuations of protein during simulation that were 0.1 to 0.51 nm, 0.07 to 0.33 nm, and 0.06 to 0.28 nm showed the fluctuation occurring in residues between 16 and 45, 98 to 131, and 211 to 276, respectively, and which are not known to have special functional relevance.

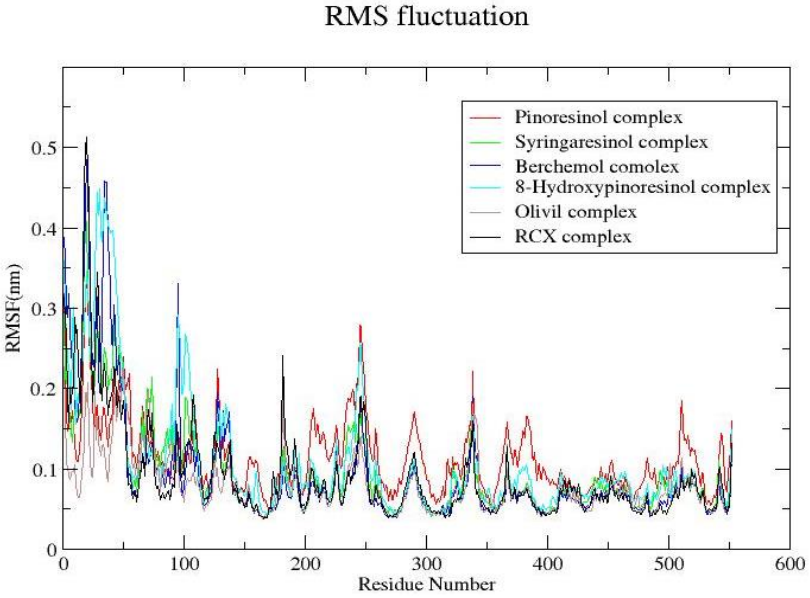

Figure 6. Root Mean Square Fluctuations (RMSF) graph of pinoresinol, syringaresinol, berchemol, 8-Hydroxypinoresinol, (-)-Olivil, and rofecoxib complexes at different time scales.

To explore the stability of the binding pocket during the MD simulation process, the root-mean-square fluctuation (RMSF) of all residues around the ligands was also calculated. In almost all complexes, the RMSF of each residue surrounding the ligand is less than 0.15 nm, as shown in Table 4, designating that the binding pocket remains stable during the MD simulation. This narrow range of RMSFs of the active site residues of these compounds demonstrated that the molecules were able to establish stable interactions with the protein during MD simulation.

Table 4. Residues of the binding pocket and their RMSF values (nm).

Residues	1	2	3	4	5	6	7
His-90	0.11	0.08	0.09	0.07	0.09	0.09	0.06
Arg-120	0.09	0.12	0.09	0.08	0.13	0.12	0.06
Gln-192	0.11	0.05	0.13	0.05	0.09	0.05	0.05
Val-349	0.10	0.05	0.08	0.05	0.05	0.05	0.04
Ser-353	0.09	0.07	0.11	0.06	0.08	0.06	0.04
Tyr-355	0.10	0.09	0.10	0.07	0.09	0.07	0.06
Tyr-385	0.05	0.05	0.06	0.04	0.06	0.05	0.04
Arg-513	0.09	0.06	0.08	0.05	0.06	0.06	0.05
Ile-517	0.09	0.05	0.10	0.04	0.09	0.04	0.04
Phe-518	0.09	0.05	0.08	0.04	0.10	0.04	0.04
Met-522	0.09	0.07	0.07	0.05	0.06	0.05	0.05
Val-523	0.08	0.07	0.07	0.05	0.06	0.06	0.05
Ser-530	0.09	0.08	0.07	0.05	0.10	0.07	0.04

1, 2, 3, 4, 5, 6, and **7** systems for pinoresinol, syringaresinol , 1-acetoxypinoresinol, berchemol, 8-hydroxypinoresinol and (-)-olivil, respectively.

3.6.3. Solvent accessible surface area (SASA)

The SASA calculation predicts the conformational changes that occurred during the interactions and whether the lignins remain embedded in the COX-2 protein. Figure 7 shows a graphical representation of the variation of SASA values as a function of time for all lignin systems. The average SASA values obtained are 239.97 ± 3.34 nm2 for the pinoresinol system, 245.97 ± 3.15 nm2 for the syringaresinol system, 237.96 ± 3.36 nm2 for the 1-Acetoxypinoresinol system, 243, 50 ± 5.51 nm2 for the berchemol system, 246.65 ± 4.91 nm2 for the 8-hydroxypinoresinol system, 235.21 ± 2.94 nm2 for the (-)-Olivil system and 240.13 ± 3.71 nm2 for the rofecoxib system. Although the difference between the SASA values obtained for all the lignin systems is not significant, the SASA values obtained show that the (-)- olivil and 1-Acetoxypinoresinol systems are the least exposed to the aqueous solvent during the MD simulations, indicating that these systems are predicted to be relatively more stable in nature than the other systems.

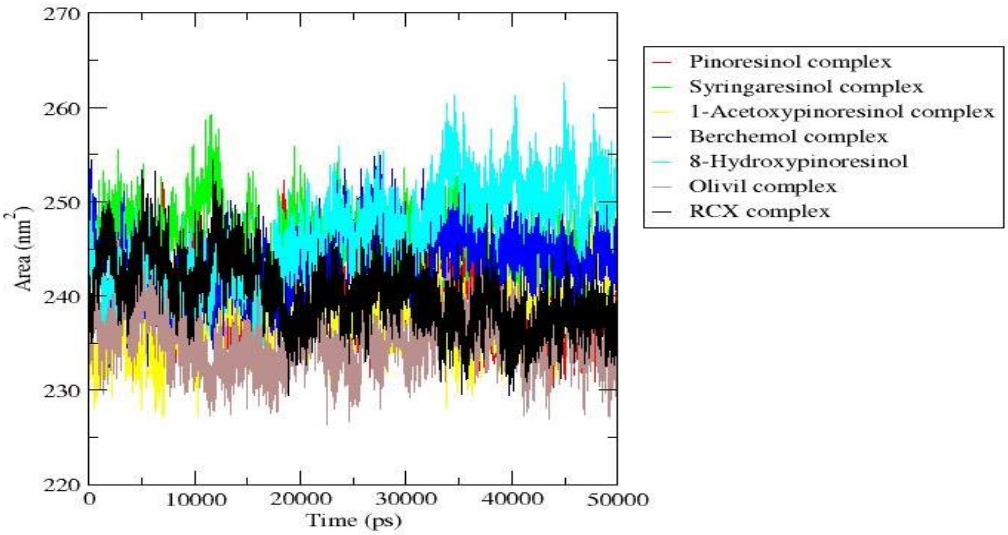

Figure 7. The plot of SASA value vs. time for pinoresinol, (-)-Olivil and berchemol complexes.

3.6.4. Comparison of lignans and rofecoxib before and after MD simulation.

To investigate the conformational rearrangements of the ligands before and after MD simulations, MD modeling has opened up many new aspects of various specific target-ligand contacts accumulated over time. A representation showing the binding site docked ligands and ligands at the last snapshot of the MD simulation was studied to analyze a new type of binding compared to their original structures. Pass from a rigid protein structure from molecular docking to MD simulation allows for thermal fluctuations. Thus changes in the side chain of residues or even larger structural rearrangements can occur in the protein. The rearrangement of the compound can also be affected by the number of rotational bonds. Therefore, the placement of the ligand can be altered, and the results can be very different from those obtained from the docking study. Visual inspection of the last conformation of the trajectory of all compounds showed that the compounds under study remain in the binding pocket. However, berchemol, 8-Hydroxypinoresinol, and (-)-olivil show more relevant changes during the MD trajectory, as shown in Figure 8, while pinoresinol, syringaresinol, and 1-acetoxypinoresinol were more stable in their conformations after the molecular dynamics simulation.

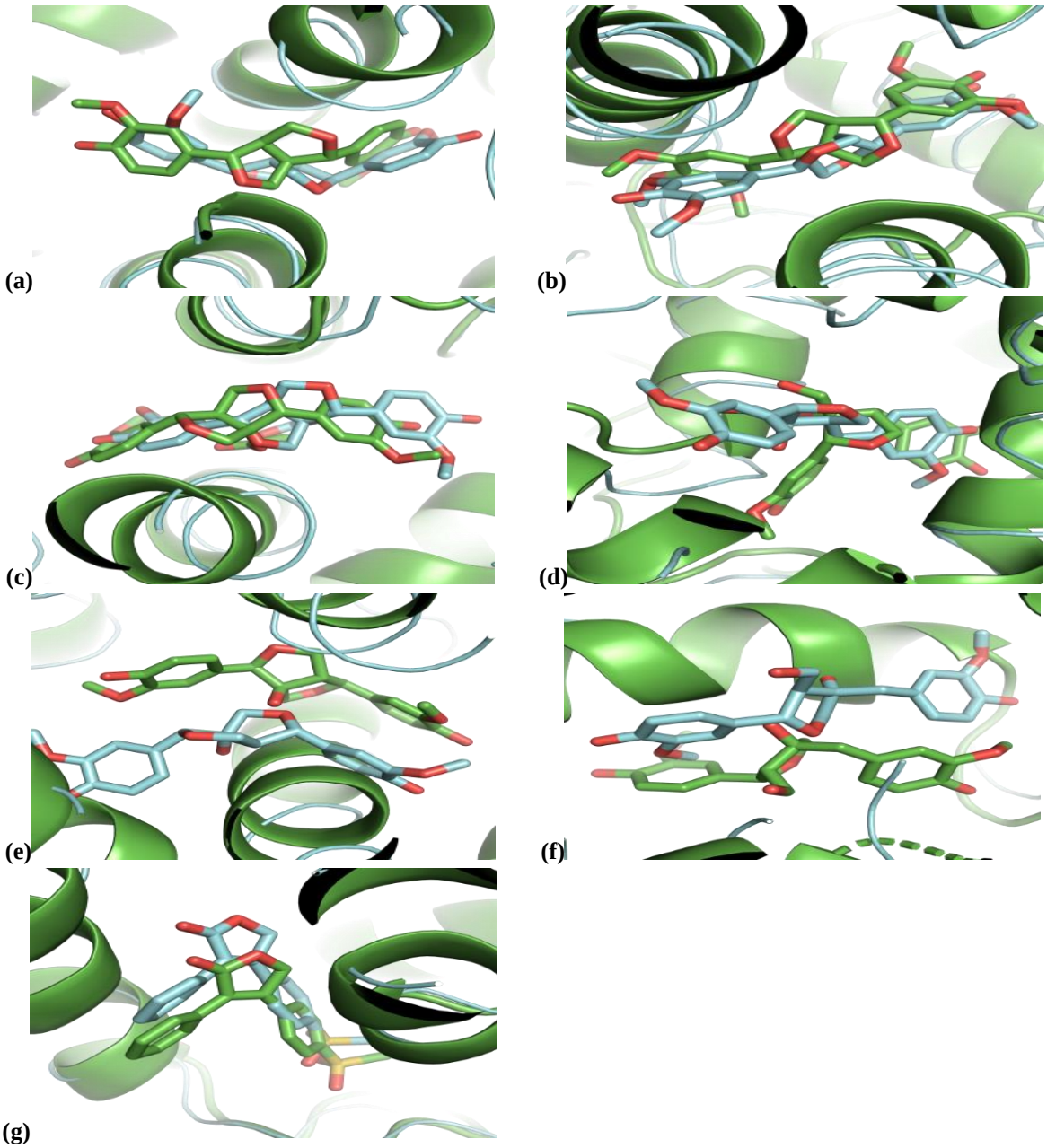

Figure 8. The conformations of compounds before in green, and after simulation in blue: A for pinoresinol complex (a), syringaresinol complex (b), berchemol complex (c), 8-Hydroxypinoresinol complex (d), (-)-Olivil complex (e) and rofecoxib complex (f).

3.6.5. Hydrogen bond analysis

Hydrogen bonding between a protein and compounds provides directionality and specificity of the interaction, which is an important aspect of molecular recognition [62]. Figure 9 shows that the number of hydrogen bonds varies between 2 and 3 for pinoresinol, syringaresinol, and berchemol, and between 1 and 4 for 8-Hydroxypinoresinol and (-)-Olivil. For the sake of comparison, rofecoxib can form as many as 2 hydrogen bonds, although they are formed only transiently during the MD simulation.

During the MD simulations, the hydrogen bonds formed in the last snapshot of the simulation for all compounds were different from the docking result, as shown in Table 5, reflecting the occurrence of structural rearrangements of the ligands during the simulations.

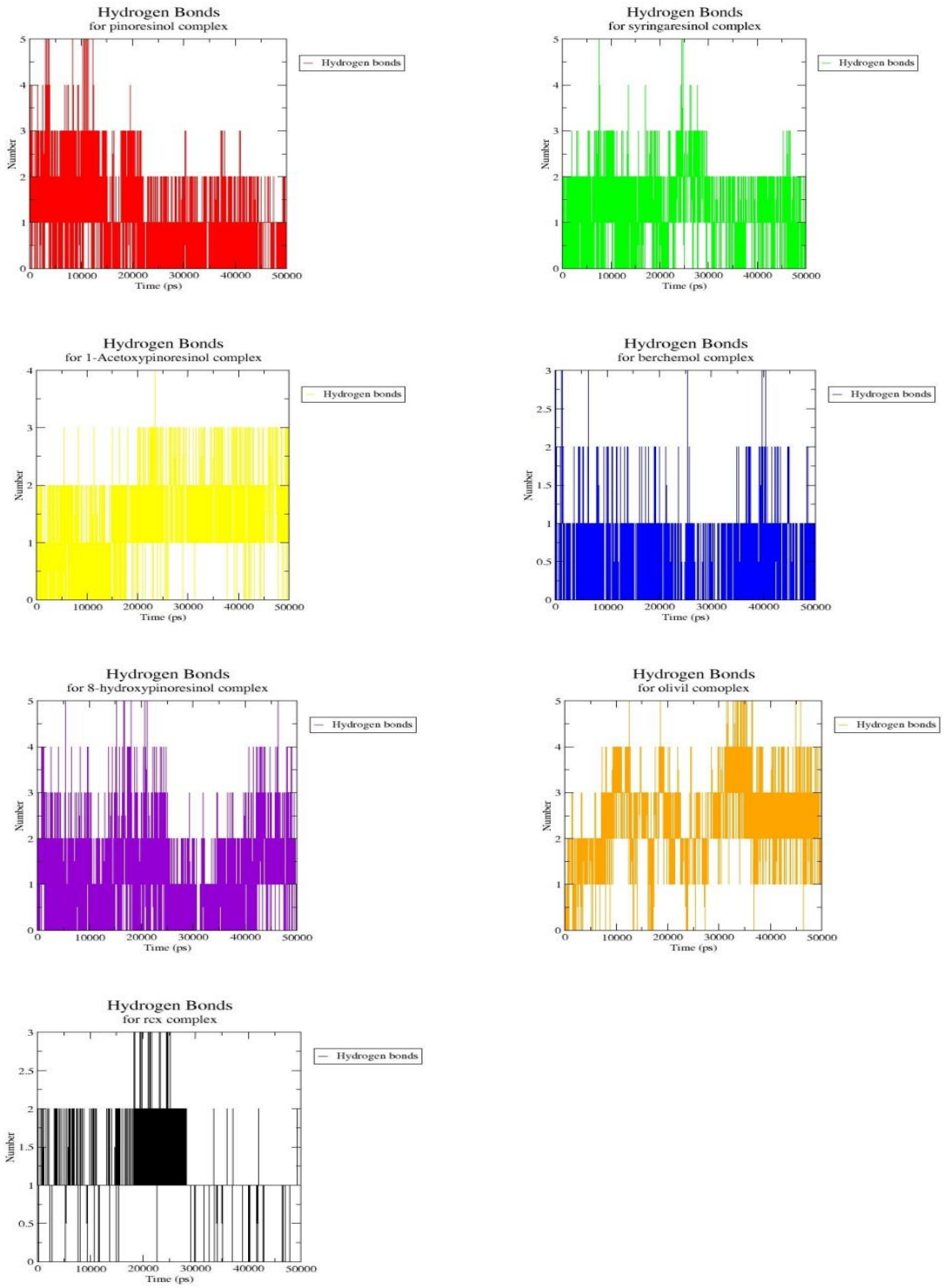

Figure 9. Number of hydrogen bonds formed for the trajectory of MD simulation for all systems.

Table 5. Hydrogen bonds analysis for all lignins and rofecoxib in the last snapshot of MD simulations.

Complexes	**H-bonds**		**Distance (Å)**
	Interacting amino acids	**Type**	
Pinoresinol	Leu-384	C=O….O-H	2.0
	Trp-387	N-H….O-H	2.0
Syringaresinol	Tyr-355	C-O….O-H	2.6
	Ser-530	H-O…..H-O	1.9
1-Acetoxypinoresinol	Ser-530	O-H….O=C	3.2
Berchemol	-	-	-
8-Hydroxypinoresinol	Ser-530	H-O…..H-O	2.4

Complexes	H-bonds		Distance (Å)
	Interacting amino acids	Type	
(-)-Olivil	Gly-519	C=O….O-H	1.7
	Glu-524	O-C=O….O-H	1.6
Rofecoxib	Arg-513	H-N-H….O=S	1.9

Results indicated in Table 5 show that among the lignins studied, syringaresinol and (-)-olivil established more favorable interactions than rofecoxib. Syringaresinol is fixed in the COX-2 active site by Tyr-355 and stabilized by Ser-530, whereas (-)-olivil interacted with Gly-519 and Glu-524, lateral pocket residues. The results for rofecoxib show that it interacted with the COX-2 active site with only Agr-513, a lateral pocket residue.

3.7. Binding energy calculation using MM-PBSA method and energetic contribution of individual residues

Based on the MD simulations, binding free energy scores for each protein-ligand complex's was calculated using the g_mmpbsa tool considering 100 frames from the last 10 ns of MD production simulation. The Molecular Mechanics Poisson–Boltzmann Surface Area (MMPBSA) method can decode significant conformational fluctuations and entropic contributions to the binding energy. In general, the binding free energy (G_{Bind}) between a protein and a ligand in the solvent can be expressed as:

$$\Delta G_{Bind} = G_{Complex} - (G_{Protein} + G_{Ligand})$$

Where $G_{Complex}$ is the total free energy of the protein-ligand complex, and $G_{Protein}$ and G_{Ligand} are the total free energies of the separated protein and ligand in a solvent, respectively.

Moreover, the protein-ligand bond strength is calculated by the magnitude of the negative binding energy. The negative values with high magnitude show a powerful binding between ligand and protein. As illustrated in Table 6, the binding energy score of all compounds is below zero and shows a good affinity for the COX-2 enzyme. Van der Waal energy, electrostatic energy, and non-polar energy (SASA energy) contribute negatively to the binding energy score, whereas polar energy contributes positively. Interestingly, syringaresinol complexes presented the least negative binding energy score of -154.06 ± 15.08 kJ/mol respectively, compared to the control rofecoxib (-146.23 ± 11.3 kJ/mol), which indicates that this molecule is more potent than the existing inhibitor, followed with pinoresinol with the binding energy of -153.41±12.41 kJ/mol. Whereas 8-Hydroxypinoresinol, (-)-Olivil, and berchemol complexes showed a high negative binding energy score compared to the control rofecoxib, with the binding energies scores of -90.46 ± 17.68 kJ/mol, -99.69 ± 31.71 kJ/mol and -104.55±15.51 kJ/mol respectively. The difference between the binding affinities predicted by the molecular docking study and MD simulation is due to the new binding mode of these ligands and their lack of rearrangement along the MD as described previously. On the other hand, different energy terms influencing the evaluation of the binding free energy score showed that in all the investigated complexes, the van der Waals energy waste driving component contributed significantly to strengthening the binding mode. The polar solvation energy had no favorable contribution to the total interaction in all the docked complexes. The electrostatic, SASA, and non-polar solvation energies similarly affect the binding free energy. Consequently, van der Waals interactions could be implied as the main driving force for the molecular recognition of COX-2 by the selected ligands.

Table 6.Van der Waal, electrostatic, polar salvation, SASA, and total binding energy for the Protein-ligand complexes.

Complexes	E_{VDW} (kJ/mol)	E_{ele} (kJ/mol)	E_{pol} (kJ/mol)	E_{SASA}(kJ/mol)	E_{l} (kJ/mol)
Syringaresinol	-193.36±10.44	-67.20±15.65	129.09±9.48	-22.58±0.80	-154.06±15.08
Pinoresinol	-195.26±10.25	-56.51±13.8	118.60±6.44	-20.24±0.66	-153.41±12.41
Rofecoxib	-181.97±10.4	-94.71±11.1	147.64± 7.0	-17.19±0.6	-146.23±11.3
Berchemol	-166.41±8.65	-27.31±9.97	110.50±14.23	-21.33±0.71	-104.55±15.51
1-hydroxyinoresinol	-172.74±9.17	-20.71±12.25	102.86±5.82	-22.90±0.72	-113.49±12.39
(-)-Olivil	-142.2±48.42	-114.38±43.0	176.42±64.11	-19.48±6.28	-99.69±31.71
8-hydroxypinoresinol	-159.8±10.79	-43.25±27.12	134.39±13.52	-21.74±0.81	-90.46±17.68

E_{VDW}: Van Der Waals energy; **E_{ele}**: Electrostaticenergy; **E_{pol}**: Polar energy; **E_{SASA}**: SASA energy.

This study has employed the chemical structure of coxibs to screen for drug candidates to inhibit COX-2 activity. Six lignin candidates, with an important structure, have been tested for their anti-inflammatory activity against COX-2 protein. The results showed that syringaresinol was the best candidate among the six lignins. It could enter to COX-2 active site and interact with the key residues with binding energy even better than the selective drug rofecoxib (-154.06±15.08 kJ/mol).

Previous studies have suggested that syringaresinol has been reported to more strongly inhibit pro-inflammatory molecules such as prostaglandin E2[63]. On the other hand, syringaresinol was demonstrated to be a potential lead compound for cosmeceutical development against UVA-induced photoaging.[64]. Else syringaresinol significantly reduced lipopolysaccharide (LPS)-induced production of interleukin-6, tumor necrosis factor α, interleukin-1 beta, cycloxygenase-2 (COX-2), and nitric oxide (NO) in BV2 microglia cells. (-)-syringaresinol also significantly reduced M1 marker CD40 expression and increased M2 marker CD206 expression. Moreover, it was found that (-)-syringaresinol inhibited LPS-induced NF-κBactivation by suppressing NF-κB p65 translocation into the nucleus in a concentration-dependent manner [65]. All these data suggest that this compound will be a very good candidate to inhibit COX-2 activity.

4. Conclusions

Most natural compounds showed moderate inhibitory activity against COX-2 inhibitory activity. The coupling between lignins and coxibs structure is a new method to find out natural compounds presenting high selectivity to inhibit COX-2 activity. The research process successfully identified six lignins against COX-2 protein (pinoresinol, syringaresinol, 1-acetoxypinoresinol, berchemol, 8-Hydroxypinoresinol and (-)-Olivil. All identified compounds were tested for the rule of five and ADME properties. The pharmacokinetic screening revealed that all of them can be used as drug molecules. The efficiency and strength of the selected lignins were further analyzed by performing a molecular docking study, which revealed successful docking results with COX-2. We conclude from the obtained results that only syringaresinol forms a stable complex with COX-2 enzyme, with evidence that the only selected compound accomplished all analyses successfully with an excellent binding energy score of -154.06±15.08kJ/mol. Therefore, the present work is a basis for the development of syringaresinol as an effective anti-inflammatory drug acting through the inhibition of an inflammatory enzymatic target, COX-2. The identification of selective COX-2 inhibitors will be subject to further computationally assisted structural optimization to improve its potency and selectivity for COX-2.

Funding

This research received no external funding

Acknowledgments

We would like to thank Francisco Javier Luque Garriga, Professor in the Department of Chemical Physics of the University of Barcelona, Spain, for his assistance. His contribution is sincerely appreciated and gratefully acknowledged, and we would like to express our deep appreciation. This research was supported through computational resources of HPC-MARWAN (www.marwan.ma/hpc) provided by the National Center for Scientific and Technical Research (CNRST), Rabat, Morocco.

Conflicts of Interest

The authors declare that they have no conflicts of interest with the contents of this article.

Reference

1. Ruslin, R.; Yamin, Y.; Kasmawati, H.; Mangrura, S.; Kadidae, L.; Armid, A.; Arba, M. The Search for Cyclooxygenase-2 (COX-2) Inhibitors for the Treatment of Inflammation Disease: An in-Silico Study. *JMDH* **2022**, *15*, 783–791, https://doi.org/10.2147/jmdh.s359429.
2. Li, X.; Teng, L.; Yang, Z. Editorial: From Chronic Inflammation to Cancer: How Far Can Immunotherapy Go? *Front. Pharmacol.* **2022**, *12*, 838917, https://doi.org/10.3389/fphar.2021.838917.
3. Gandhi, J.; Khera, L.; Gaur, N.; Paul, C.; Kaul, R. Role of Modulator of Inflammation Cyclooxygenase-2 in Gammaherpesvirus Mediated Tumorigenesis. *Front Microbiol.* **2017**, *8*, 538, https://doi.org/10.3389/fmicb.2017.00538.
4. Tai, F.W.D.; McAlindon, M.E. Non-Steroidal Anti-Inflammatory Drugs and the Gastrointestinal Tract. *Clin Med* **2021**, *21*, 131–134, https://doi.org/10.7861/clinmed.2021-0039.
5. Ghazanfari, N.; Waarde, A.; Dierckx, R.A.J.O.; Doorduin, J.; Vries, E.F.J. Is Cyclooxygenase-1 Involved in Neuroinflammation? *J Neurosci Res* **2021**, *99*, 2976–2998, https://doi.org/10.1002/jnr.24934.
6. Miciaccia, M.; Belviso, B.D.; Iaselli, M.; Cingolani, G.; Ferorelli, S.; Cappellari, M.; Loguercio Polosa, P.; Perrone, M.G.; Caliandro, R.; Scilimati, A. Three-Dimensional Structure of Human Cyclooxygenase (*h*COX)-1. *Sci Rep* **2021**, *11*, 4312, https://doi.org/10.1038/s41598-021-83438-z.
7. Vane, J.R.; Bakhle, Y.S.; Botting, R.M. Cyclooxygenases 1 and 2. *Annu Rev Pharmacol Toxicol.* **1998**, *38*, 97–120, https://doi.org/10.1146/annurev.pharmtox.38.1.97.
8. Chokshi, R.; Bennett, O.; Zhelay, T.; Kozak, J.A. NSAIDs Naproxen, Ibuprofen, Salicylate, and Aspirin Inhibit TRPM7 Channels by Cytosolic Acidification. *Front. Physiol.* **2021**, *12*, 727549, https://doi.org/10.3389/fphys.2021.727549.
9. Machado, G.C.; Abdel-Shaheed, C.; Underwood, M.; Day, R.O. Non-Steroidal Anti-Inflammatory Drugs (NSAIDs) for Musculoskeletal Pain. *BMJ* **2021**, *372*, n104, https://doi.org/10.1136/bmj.n104.
10. Inotai, A.; Hankó, B.; Mészáros, A. Trends in the Non-Steroidal Anti-Inflammatory Drug Market in Six Central-Eastern European Countries Based on Retail Information. *Pharmacoepidemiol Drug Saf* **2010**, *19*, 183–190, http://dx.doi.org/10.1002/pds.1893.
11. Meade, E.A.; Smith, W.L.; DeWitt, D.L. Differential Inhibition of Prostaglandin Endoperoxide Synthase (Cyclooxygenase) Isozymes by Aspirin and Other Non-Steroidal Anti-Inflammatory Drugs. *J Biol Chem* **1993**, *268*, 6610–6614.
12. Ju, Z.; Li, M.; Xu, J.; Howell, D.C.; Li, Z.; Chen, F.-E. Recent Development on COX-2 Inhibitors as Promising Anti-Inflammatory Agents: The Past 10 Years. *Acta Pharmaceutica Sinica B* **2022**, *12*, 2790-2807, https://doi.org/10.1016/j.apsb.2022.01.002.
13. Prasit, P.; Wang, Z.; Brideau, C. et al. The Discovery of Rofecoxib, [MK 966, Vioxx, 4-(4'-Methylsulfonylphenyl)-3-Phenyl-2(5H)-Furanone], an Orally Active Cyclooxygenase-2-Inhibitor. *Bioorg Med Chem Lett* **1999**, *9*, 1773–1778, https://doi.org/10.1016/S0960-894X(99)00288-7.

14. Burayk, S.; Oh-hashi, K.; Kandeel, M. Drug Discovery of New Anti-Inflammatory Compounds by Targeting Cyclooxygenases. *Pharmaceuticals* **2022**, *15*, 282, https://doi.org/10.3390/ph15030282.
15. Luong, C.; Miller, A.; Barnett, J.; Chow, J.; Ramesha, C.; Browner, M.F. Flexibility of the NSAID Binding Site in the Structure of Human Cyclooxygenase-2. *Nat Struct Biol* **1996**, *3*, 927–933, https://doi.org/10.1038/nsb1196-927.
16. Kurumbail, R.G.; Stevens, A.M.; Gierse, J.K. et al. Structural Basis for Selective Inhibition of Cyclooxygenase-2 by Anti-Inflammatory Agents. *Nature* **1996**, *384*, 644–648, https://doi.org/10.1038/384644a0.
17. Orlando, B.J.; Malkowski, M.G. Crystal Structure of Rofecoxib Bound to Human Cyclooxygenase-2. *Acta Crystallogr F Struct Biol Commun*. **2016**, *72*, 772–776, https://doi.org/10.1107/S2053230X16014230.
18. Sooriakumaran, P. COX-2 Inhibitors and the Heart: Are All Coxibs the Same? *Postgraduate Medical Journal* **2006**, *82*, 242–245, https://doi.org/10.1136/pgmj.2005.042234.
19. Walter, M.F.; Jacob, R.F.; Day, C.A.; Dahlborg, R.; Weng, Y.; Mason, R.P. Sulfone COX-2 Inhibitors Increase Susceptibility of Human LDL and Plasma to Oxidative Modification: Comparison to Sulfonamide COX-2 Inhibitors and NSAIDs. *Atherosclerosis* **2004**, *177*, 235–243, https://doi.org/10.1016/j.atherosclerosis.2004.10.001.
20. Mason, R.P.; Walter, M.F.; Day, C.A.; Jacob, R.F. A Biological Rationale for the Cardiotoxic Effects of Rofecoxib: Comparative Analysis with Other COX-2 Selective Agents and NSAids. *Subcell Biochem* **2007**, *42*, 175–190.
21. Preston Mason, R.; Walter, M.F.; McNulty, H.P.; Lockwood, S.F.; Byun, J.; Day, C.A.; Jacob, R.F. Rofecoxib Increases Susceptibility of Human LDL and Membrane Lipids to Oxidative Damage: A Mechanism of Cardiotoxicity: *Journal of Cardiovascular Pharmacology* **2006**, *47*, S7–S14, https://doi.org/10.1097/00005344-200605001-00003.
22. Dogné, J.-M.; Supuran, C.T.; Pratico, D. Adverse Cardiovascular Effects of the Coxibs. *J. Med. Chem.* **2005**, *48*, 2251–2257, https://doi.org/10.1021/jm0402059.
23. Zarghi, A.; Arfaei, S. Selective COX-2 Inhibitors: A Review of Their Structure-Activity Relationships. *Iran J Pharm Res* **2011**, *10*, 655–683.
24. Owen, M.C.; Szó´ri, M.; Jojárt, B.; Viskolcz, B.; Csizmadia, I.G. Conformational and Thermodynamic Analysis of the COXIB Scaffold Using Quantum Chemical Calculations. *Int. J. Quantum Chem.* **2012**, *112*, 922–936, https://doi.org/10.1002/qua.23049.
25. During, A.; Debouche, C.; Raas, T.; Larondelle, Y. Among Plant Lignans, Pinoresinol Has the Strongest Anti-inflammatory Properties in Human Intestinal Caco-2 Cells. *J Nutr.* **2012**, *142*, 1798–1805, doi:10.3945/jn.112.162453.
26. Jung, H.-J.; Park, H.-J.; Kim, R.-G.; Shin, K.-M.; Ha, J.; Choi, J.-W.; Kim, H.J.; Lee, Y.S.; Lee, K.-T. In Vivo Anti-Inflammatory and Antinociceptive Effects of Liriodendrin Isolated from the Stem Bark of Acanthopanax Senticosus. *Planta Med* **2003**, *69*, 610–616, https://doi.org/10.1055/s-2003-41127.
27. Kim, K.-W.; Yoon, C.-S.; Park, S.-J.; Bae, G.-S.; Kim, D.-G.; Kim, Y.-C.; Oh, H. Chemical Analysis of the Ingredients of 20% Aqueous Ethanol Extract of *Nardostachys Jatamansi* through Phytochemical Study and Evaluation of Anti-Neuroinflammatory Component. *Evidence-Based Complementary and Alternative Medicine* **2021**, *2021*, 5901653, https://doi.org/10.1155/2021/5901653.
28. Menendez, J.A.; Vazquez-Martin, A.; Garcia-Villalba, R.; Carrasco-Pancorbo, A.; Oliveras-Ferraros, C.; Fernandez-Gutierrez, A.; Segura-Carretero, A. TabAnti-HER2 (ErbB-2) Oncogene Effects of Phenolic Compounds Directly Isolated from Commercial Extra-Virgin Olive Oil (EVOO). *BMC Cancer* **2008**, *8*, 377, https://doi.org/10.1186/1471-2407-8-377.
29. Li, W.; Kim, J.H.; Zhou, W.; Shim, S.H.; Ma, J.Y.; Kim, Y.H. Soluble Epoxide Hydrolase Inhibitory Activity of Phenolic Components from the Rhizomes and Roots of Gentiana Scabra. *Biosci Biotechnol Biochem* **2015**, *79*, 907–911, https://doi.org/10.1080/09168451.2014.1002451.
30. Magoulas, G.E.; Papaioannou, D. Bioinspired Syntheses of Dimeric Hydroxycinnamic Acids (Lignans) and Hybrids, Using Phenol Oxidative Coupling as Key Reaction, and Medicinal Significance Thereof. *Molecules* **2014**, *19*, 19769–19835, https://doi.org/10.3390/molecules191219769.
31. Spiridon, I. BIOLOGICAL AND PHARMACEUTICAL APPLICATIONS OF LIGNIN AND ITS DERIVATIVES: A MINI-REVIEW. *Cellulose Chem. Technol* **2018**, *52*, 543–550.
32. Christoph, T.; Buschmann, H. Cyclooxygenase Inhibition: From NSAIDS to Selective COX-2 Inhibitors (Part 3). *In: Buschmann, H.; Christoph, T.; Maul, C.; Sundermann, B. (Eds.), Analgesics.* Wiley-VCH Verlag GmbH & Co. KGaA, Weinheim **2005**, https://doi.org/10.1002/3527605614.ch2c.

33. Domínguez-Robles, J.; Carcamo-Martinez, A.; Stewart, S.A.; Donnelly, R.F.; Larraneta, E.; Borrega, M. Lignin for Pharmaceutical and Biomedical Applications – Could this become a reality? ***Sustainable Chemistry and Pharmacy*** **2020,** ***18,*** **100320,** https://doi.org/10.1016/j.scp.2020.100320**.**
34. Miranda, I.; Simões, R.; Medeiros, B.; Nampoothiri, K.M.; Sukumaran, R.K.; Rajan, D.; Pereira, H.; Ferreira-Dias, S. Valorization of Lignocellulosic Residues from the Olive Oil Industry by Production of Lignin, Glucose and Functional Sugars. *Bioresource Technology* **2019**, *292*, 121936, https://doi.org/10.1016/j.biortech.2019.121936.
35. Veber, D.F.; Johnson, S.R.; Cheng, H.-Y.; Smith, B.R.; Ward, K.W.; Kopple, K.D. Molecular Properties That Influence the Oral Bioavailability of Drug Candidates. *J Med Chem* **2002**, *45*, 2615–2623, https://doi.org/10.1021/jm020017n.
36. Turner, J.V.; Agatonovic-Kustrin, S. In Silico Prediction of Oral Bioavailability. *In: Taylor, J.B.; Triggle, D.J. (Eds.), Comprehensive Medicinal Chemistry II*. Elsevier **2007**.
37. Laskowski, R.A.; Swindells, M.B. LigPlot+: Multiple Ligand-Protein Interaction Diagrams for Drug Discovery. *J Chem Inf Model* **2011**, *51*, 2778–2786, https://doi.org/10.1021/ci200227u.
38. Kumar, S.S.; T, A. In Silico Design And Molecular Docking Studies Of Some 1, 2-Benzisoxazole Derivatives For Their Analgesic And Anti-Inflammatory Activity. *Int J Curr Pharm Sci* **2017**, *9*, 133, http://dx.doi.org/10.22159/ijcpr.2017.v9i3.18886.
39. Deb, S.; Reeves, A.A.; Hopefl, R.; Bejusca, R. ADME and Pharmacokinetic Properties of Remdesivir: Its Drug Interaction Potential. *Pharmaceuticals* **2021**, *14*, 655, https://doi.org/10.3390/ph14070655.
40. Mandlik, V.; Bejugam, P.R.; Singh, S. Application of Artificial Neural Networks in Modern Drug Discovery. *In: Puri, M.; Pathak, Y.; Sutariya, V.K.; Tipparaju, S.; Moreno, W. (Eds.). Artificial Neural Network for Drug Design, Delivery and Disposition*, Elsevier **2016**, https://doi.org/10.1016/C2014-0-00253-5.
41. Hidalgo, I.J.; Raub, T.J.; Borchardt, R.T. Characterization of the Human Colon Carcinoma Cell Line (Caco-2) as a Model System for Intestinal Epithelial Permeability. *Gastroenterology* **1989**, *96*, 736–749.
42. Artursson, P.; Palm, K.; Luthman, K. Caco-2 Monolayers in Experimental and Theoretical Predictions of Drug Transport. *Adv Drug Deliv Rev* **2001**, *46*, 27–43, https://doi.org/10.1016/s0169-409x(00)00128-9.
43. Press, B.; Di Grandi, D. Permeability for Intestinal Absorption: Caco-2 Assay and Related Issues. *Curr Drug Metab* **2008**, *9*, 893–900, https://doi.org/10.2174/138920008786485119.
44. Norinder, U.; Haeberlein, M. Computational Approaches to the Prediction of the Blood-Brain Distribution. *Adv Drug Deliv Rev* **2002**, *54*, 291–313, https://doi.org/10.1016/S0169-409X(02)00005-4.
45. Li, H.; Yap, C.W.; Ung, C.Y.; Xue, Y.; Cao, Z.W.; Chen, Y.Z. Effect of Selection of Molecular Descriptors on the Prediction of Blood-Brain Barrier Penetrating and Nonpenetrating Agents by Statistical Learning Methods. *J Chem Inf Model* **2005**, *45*, 1376–1384, https://doi.org/10.1021/ci050135u.
46. Cecchelli, R.; Berezowski, V.; Lundquist, S.; Culot, M.; Renftel, M.; Dehouck, M.-P.; Fenart, L. Modelling of the Blood-Brain Barrier in Drug Discovery and Development. *Nat Rev Drug Discov* **2007**, *6*, 650–661, https://doi.org/10.1038/nrd2368.
47. Reichel, A. Addressing Central Nervous System (CNS) Penetration in Drug Discovery: Basics and Implications of the Evolving New Concept. *Chem Biodivers* **2009**, *6*, 2030–2049, https://doi.org/10.1002/cbdv.200900103.
48. Lynch, T.; Price, A. The Effect of Cytochrome P450 Metabolism on Drug Response, Interactions, and Adverse Effects. *Am Fam Physician* **2007**, *76*, 391-396.
49. Nembri, S.; Grisoni, F.; Consonni, V.; Todeschini, R. *In Silico* Prediction of Cytochrome P450-Drug Interaction: QSARs for CYP3A4 and CYP2C9. *IJMS* **2016**, *17*, 914, https://doi.org/10.3390/ijms17060914.
50. Pea, F. Principles of Pharmacodynamics and Pharmacokinetics of Drugs Used in Extracorporeal Therapies. *In: Ronco, C.; Kellum, J.A. (Eds.) Critical Care Nephrology*. Elsevier **2019**, https://doi.org/10.1016/C2015-0-00412-9.
51. Sams, R.A.; Muir, W.W. Principles of Drug Disposition and Drug Interaction in Horses. *In: Muir, W.W.; Hubbell, J.A.E. (Eds.) Equine Anesthesia*. Elsevier **2009**, https://doi.org/10.1016/B978-1-4160-2326-5.X0001-6.
52. Cole, J.C.; Murray, C.W.; Nissink, J.W.M.; Taylor, R.D.; Taylor, R. Comparing Protein-Ligand Docking Programs Is Difficult. *Proteins* **2005**, *60*, 325–332, https://doi.org/10.1002/prot.20497.
53. Gouda, A.; Ali, H.; Almalki, W.; Azim, M.; Abourehab, M.; Abdelazeem, A. Design, Synthesis, and Biological Evaluation of Some Novel Pyrrolizine Derivatives as COX Inhibitors with Anti-Inflammatory/Analgesic Activities and Low Ulcerogenic Liability. *Molecules* **2016**, *21*, 201, https://doi.org/10.3390/molecules21020201.

54. Kothekar, V.; Sahi, S.; Srinivasan, M.; Mohan, A.; Mishra, J. Recognition of Cyclooxygenase-2 (COX-2) Active Site by NSAIDs: A Computer Modelling Study. *Indian J Biochem Biophys* **2001**, *38*, 56–63.
55. Marnett, L.J.; Rowlinson, S.W.; Goodwin, D.C.; Kalgutkar, A.S.; Lanzo, C.A. Arachidonic Acid Oxygenation by COX-1 and COX-2. Mechanisms of Catalysis and Inhibition. *J Biol Chem* **1999**, *274*, 22903–22906, https://doi.org/10.1074/jbc.274.33.22903.
56. Thuresson, E.D.; Lakkides, K.M.; Rieke, C.J.; Sun, Y.; Wingerd, B.A.; Micielli, R.; Mulichak, A.M.; Malkowski, M.G.; Garavito, R.M.; Smith, W.L. Prostaglandin Endoperoxide H Synthase-1: The Functions of Cyclooxygenase Active Site Residues in the Binding, Positioning, and Oxygenation of Arachidonic Acid. *J Biol Chem* **2001**, *276*, 10347–10357, https://doi.org/10.1074/jbc.m009377200.
57. Kritikou, E.; Kalogiouri, N.P.; Kostakis, M et al. Geographical Characterization of Olive Oils from the North Aegean Region Based on the Analysis of Biophenols with UHPLC-QTOF-MS. *Foods* **2021**, *10*, 2102, https://doi.org/10.3390/foods10092102.
58. Hashmi, M.A.; Khan, A.; Hanif, M.; Farooq, U.; Perveen, S. Traditional Uses, Phytochemistry, and Pharmacology of Olea Europaea (Olive). *Evid Based Complement Alternat Med* **2015**, *2015*, 541591, https://doi.org/10.1155/2015/541591.
59. Price, M.L.; Jorgensen, W.L. Rationale for the Observed COX-2/COX-1 Selectivity of Celecoxib from Monte Carlo Simulations. *Bioorg Med Chem Lett* **2001**, *11*, 1541–1544, https://doi.org/10.1016/S0960-894X(00)00522-9.
60. Llorens, O.; Perez, J.J.; Palomer, A.; Mauleon, D. Differential Binding Mode of Diverse Cyclooxygenase Inhibitors. *J Mol Graph Model* **2002**, *20*, 359–371, https://doi.org/10.1016/S1093-3263(01)00135-8.
61. Ahmadi, M.; Bekeschus, S.; Weltmann, K.-D.; von Woedtke, T.; Wende, K. Non-Steroidal Anti-Inflammatory Drugs: Recent Advances in the Use of Synthetic COX-2 Inhibitors. *RSC Med. Chem.* **2022**, *13*, 471-476, https://doi.org/10.1039/D1MD00280E.
62. Bissantz, C.; Kuhn, B.; Stahl, M. A Medicinal Chemist's Guide to Molecular Interactions. *J. Med. Chem.* **2010**, *53*, 5061–5084, https://doi.org/10.1021/jm100112j.
63. Kim, M.J.; Wang, H.S.; Lee, M.W. Anti-Inflammatory Effects of Fermented Bark of *Acanthopanax Sessiliflorus* and Its Isolated Compounds on Lipopolysaccharide-Treated RAW 264.7 Macrophage Cells. *Evidence-Based Complementary and Alternative Medicine* **2020**, *2020*, 6749425, https://doi.org/10.1155/2020/6749425.
64. Oh, J.H.; Joo, Y.H.; Karadeniz, F.; Ko, J.; Kong, C.-S. Syringaresinol Inhibits UVA-Induced MMP-1 Expression by Suppression of MAPK/AP-1 Signaling in HaCaT Keratinocytes and Human Dermal Fibroblasts. *IJMS* **2020**, *21*, 3981, https://doi.org/10.3390/ijms21113981.
65. Zhang, L.; Jiang, X.; Zhang, J.; Gao, H.; Yang, L.; Li, D.; Zhang, Q.; Wang, B.; Cui, L.; Wang, X. (−)-Syringaresinol Suppressed LPS-Induced Microglia Activation via Downregulation of NF-KB P65 Signaling and Interaction with ERβ. *International Immunopharmacology* **2021**, *99*, 107986, https://doi.org/10.1016/j.intimp.2021.107986.